Electric Power Systems Research 173 (2019) 18–28

Contents lists available at ScienceDirect

Electric Power Systems Research

journal homepage: www.elsevier.com/locate/epsr

Coordinated control for the series grid side converter-based DFIG at subsynchronous operation

Vinicius P. Suppioni, Ahda P. Grilo*, Julio C. Teixeira

Engineering, Modeling and Applied Social Sciences Center, Universidade Federal do ABC, Santo André, Brazil

ARTICLE INFO

Keywords:
Index terms – DFIG
Series grid Side converter
Power control

ABSTRACT

Connecting the Grid Side Converter of Doubly Fed Induction Generators (DFIG) in series presents some advantages compared to the traditional parallel connection. The series converter acts as a Dynamic Voltage Restorer, improving the DFIG capability to deal with disturbances in the grid, specially symmetric and asymmetric faults. However, a drawback of this scheme is to control the power during subsynchronous speeds. For this operating condition, the stator voltage should be higher than the grid voltage, which may result in machine saturation. This paper proposes a control strategy for the series-based DFIG to avoid the need of the stator voltage from being higher than the grid voltage. The proposed solution for this issue is based on phase shifts of the voltages and currents and a coordinated control, considering several wind turbines, to achieve a unity power factor at the point of common coupling of the wind farm. The proposed solution overcomes the saturation problem, as it does not depend on the stator voltage magnitude variation. The validation is performed by computational simulations using the MatLab Simulink environment.

1. Introduction

In the last two decades, the growth of the share of wind power in the world's energy production was consolidated as one of the best choices to meet growing energy demand through a renewable energy source. In 2015, a new wind power installation record was achieved, adding more 63,690 MW around the world [1]. From this period onwards, the amount of new installations was slightly reduced, comprising new 51,402 MW in 2016 and 52,552 MW in 2017. Wind energy, by the end of 2017, can supply more than 5% of the global electricity demand. For many countries, wind power has become a pillar among the strategies to phase out fossil and nuclear energy [2].

Due to its converter using only a fraction of the machine nominal power and a wide range of operational speeds, DFIG-based wind turbine was the first variable-speed wind turbine configuration widely installed, and, even nowadays, its lower cost is still an important advantage when compared to the full converter wind turbines [3,4].

The increasing penetration of wind energy worldwide has encouraged power system operators to develop grid codes to face the new challenges of this type of power plant. The grid codes requirements can be divided in two main groups related to static and dynamic operation. The static requirements comprise the load flow at the point of common coupling (PCC) for the transmission grid, while dynamic requirements comprise the expected behavior of wind turbines under fault and disturbances conditions [5].

Among the dynamic requirements, the Low-Voltage Ride-Through (LVRT) capability is considered the most challenging one for wind turbines design and manufacturing technology [6]. DFIG-based wind turbines are sensitive to grid disturbances, especially to voltage sags [7]. A voltage sag at the PCC induces high currents at the rotor and stator windings of DFIG. As the rotor converter is connected to the rotor windings, the converter is disconnected for protection, while the currents are elevated and DFIG control capability fails. Consequently, DFIG can only provide active support to the grid during or after a disturbance when its rotor protection is not enabled [8,9].

Another challenging dynamic requirement for wind turbines is the operation under unbalanced grid voltage conditions. Unbalanced three-phase conditions are common in weak grids and are caused mainly by asymmetrical loads, heavy single-phase demand, transformer windings, asymmetrical transmission impedances, and grid faults [10]. Even a low level of voltage unbalance produces oscillations in the electromagnetic torque of the DFIG and unbalances in the currents at the stator and rotor. The National Electrical Manufacturers Association (NEMA) in Standards Publication no. MG 1–1993 does not recommend operating the asynchronous machine under voltage unbalances above 5% [11].

In the last years, several solutions have been proposed for increasing

* Corresponding author.
E-mail address: ahda.pavani@ufabc.edu.br (A.P. Grilo).

https://doi.org/10.1016/j.epsr.2019.04.006
Received 18 October 2018; Received in revised form 7 March 2019; Accepted 2 April 2019

the LVRT performance of the DFIG and complying with demanding grid codes. Some of these solutions propose different control structures, for example, in Ref. [12] a heightened state-feedback predictive control structure is used to surpass the performance of the PI and PI Resonant controllers. Another solution is to employ an extra device, as for example, the STATCOM [13] or a SVC [14], which can be controlled to inject reactive power during faults to support the voltage. However, as can be seen in Ref. [13], this solution is not capable of limiting the RSC overcurrents. In this sense, current limiters can be used to limit wind park contribution to the fault current [15] or a series grid side passive impedance for damping the stator flux oscillations [16]. It has been noticed that although this is a good solution for voltage sag levels from 15%, it results in relevant peaks of electromagnetic torque [16]. Another solution is the use of series dynamic resistors, as proposed in [17], which is, on one hand, a low-cost solution, but on the other hand, the use of this solution limits the injection of reactive power from DFIG to the grid to assist the grid recovery.

Among the solutions present in literature, the use of a Dynamic Voltage Restorer (DVR) has been proposed to fully or, at least, partially compensate either voltage dips or voltage unbalances at the machine terminals [8,18–22]. The main benefit of employing DVR during disturbances is it decouples the stator voltage from the grid voltage, allowing the continuous operation of DFIG during disturbances.

Nevertheless, for a more economical solution, the DVR can be integrated into the DFIG, replacing the Grid Side Converter (GSC) and resulting in the Series DFIG configuration, as proposed in Ref. [23]. In this topology, the GSC is connected in series to the grid, using an injection transformer or capacitors, namely Series Grid Side Converter (SGSC). This configuration provides the DFIG the benefits of a DVR connected to its terminals [24–32].

For the series DFIG, the method used for processing the rotor active power is different from the one used for the conventional DFIG. As the GSC is connected in series, the machine and the converter present the same current and, as a consequence, the control of the rotor power should be based on controlling either the voltage magnitude or the phases between current and voltage of the converter and the machine.

The method found in the literature for processing the SGSC power assumes that the DFIG power factor should be kept unitary, keeping the voltage of the injection transformer connected to the SGSC aligned to the grid voltage [23,25]. As a result, the method results in stator voltage magnitude changes to allow the control of the SGSC power exchanged between the rotor circuit and the grid. However, in the subsynchronous operation, the control results in an increase of the stator voltage to absorb active power from the grid. This increase in the stator voltage may lead to the saturation of the machine stator flux. Consequently, such power processing control is not able to exchange the rotor active power to the grid using the entire range of operating speeds expected of a DFIG and, for these operating conditions, this configuration operates in suboptimal operational points related to the wind power conversion [24,25].

This drawback discouraged studies on DFIG using the series configuration. In effect, the literature available considers the DFIG operating in a narrower range of speeds [27,30,33–35]. As a consequence, the SGSC is far more present in the literature as a complementary converter than substituting the original GSC, which represents a significant increase in complexity and cost.

Therefore, the objective of this paper is to enable the full operation of the series DFIG. It is proposed a solution for controlling the power exchanged by the SGSC with the grid based on voltage and current phase shifts instead of voltage magnitude changes. The proposed solution, however, results in DFIG operating out of the Unitary Power Factor Operation - UPFO. To overcome this, it is proposed a coordinate operation of the wind farm considering a power factor compensation by controlling a pair or a group of wind turbines. To the best of our knowledge, this type of solution has not been reported in the literature.

The paper is organized as follows: Section 2 presents SGSC - based DFIG architecture, the main equations applied for modeling and the controls reported in the literature for the Rotor Side Converter – RSC and for SGSC. Section 3 comprises the proposed solution to overcome the drawback in subsynchronous speeds and Section 4 illustrates the validation of the proposed solution through the results obtained by computational simulations. Section 5 presents the main conclusions.

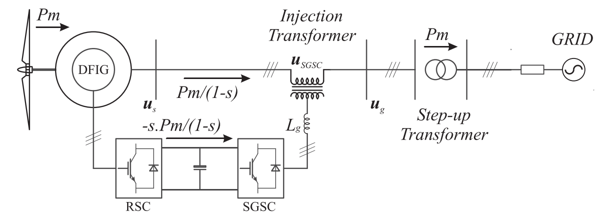

Fig. 1. Two-converters series DFIG topology.

2. System architecture, modeling and controls

Despite the different coupling method of the SGSC, DFIG operational principles and the power flow remain the same, as shown in Fig. 1.

In Fig. 1, in the two-converters series topology, SGSC is coupled to the grid by a series injection transformer. Consequently, unlike the conventional DFIG, the stator terminal voltage (Us) depends not only on the grid voltage (U_g) but also on the voltage output of SGSC (U_{SGSC}).

Furthermore, U_{SGSC} establishes the power exchanged between the grid and SGSC. SGSC power, in turn, is given by the rotor power flux of DFIG, therefore, it depends on the turbine mechanical power (P_m) and on the machine slip (s). Stator and rotor power fluxes are given by Eqs. (1) and (2), respectively:

$$P_S = \frac{P_m}{(1-s)} \tag{1}$$

$$P_R = -s\frac{P_m}{(1-s)} \tag{2}$$

As previously mentioned, SGSC voltage output is responsible for controlling the power of the back-to-back converter exchanged with the grid. Active and reactive SGSC powers are given by, respectively:

$$P_{SGSC} = U_{SGSCd}.\ I_{sd} + U_{SGSCq}.\ I_{sq} \tag{3}$$

$$Q_{SGSC} = U_{SGSCq}.\ I_{sd} - U_{SGSCd}.\ I_{sq} \tag{4}$$

where, U_{SGSCd} and U_{SGSCq} are the direct and quadrature voltage components induced by the injection transformer of SGSC, and I_{sd} and I_{sq} are the direct and quadrature components of the stator current.

Assuming a UPFO, where the stator voltage, the stator current, and DFIG voltage are aligned and according to the adopted reference, they have only the direct component ($U_{sq} = 0$, $I_{sq} = 0$, $U_{SGSCq} = 0$, $U_{gq} = 0$). The grid, quadrature voltages are given by:

$$U_{gd} = P_m/I_{sd} \tag{5}$$

$$U_{SGSCd} = P_{SGSC}/I_{sd} \tag{6}$$

$$U_{sd} = P_s/I_{sd} \tag{7}$$

Replacing (5) in (6) and (7):

$$U_{SGSCd} = (P_{SGSC}/P_m)U_{gd} \tag{8}$$

$$U_{sd} = (P_s/P_m)U_{gd} \tag{9}$$

Appling the relationship of the stator and rotor power with the slip, given by (1) and (2), the Eqs. (8) and (9) can be rewritten as, respectively:

$$U_{SGSCd} = \left(\frac{s}{1-s}\right)U_{gd} \tag{10}$$

$$U_{sd} = \left(\frac{1}{1-s}\right)U_{gd} \tag{11}$$

Where,

$$U_{gd} = U_{sd} + U_{SGSCd} \tag{12}$$

These equations reveal that the converter and the machine stator voltages assume different levels during the operation, which are following discussed.

2.1. Supersynchronous operation

The maximum operating rotor speed of a DFIG based wind turbine is 20% above the synchronous speed, which, according to (11), results in a stator voltage 17% lower than the grid voltage. A stator voltage lower than its nominal value implies a reduction of the machine flux and of the machine capacity in this operating condition.

As compensation, is possible to apply a phase shift in stator voltage through the SGSC control. Therefore, controlling the power at the super-synchronous speeds without changing the magnitude of the voltage in the machine stator, avoiding to change the machine stator flux. This control strategy keeps the unitary power factor, as the stator current is aligned with DFIG terminal voltage, as shown in Fig. 2. This solution was first presented in Ref. [25].

The method is based on controlling the quadrature component of the stator voltage (U_{sq}) to keep a unitary stator flux $|\varphi_s| = 1$. Considering a unitary grid voltage module $|U_g| = 1$, for $|\varphi_s| = 1$, the magnitude of the stator voltage (U_s) must be the same of the magnitude of the grid (U_g).

Considering the *dq* frame referenced to U_g and I_s aligned to U_g, the SGSC active power injection occurs when $U_{sd} < U_g$. Therefore, to reach a unitary module for the stator voltage, its quadrature component must be set as:

$$U_{sq} = \sqrt{1 - U_{sd}^{2}} \tag{13}$$

In this case, the quadrature component of the stator voltage (U_{sq}) is responsible for reactive power flowing from the machine stator. However, the stator current (I_s) is aligned to the grid voltage (U_g), which means that all the reactive power provided by the machine is absorbed by SGSC, as shown by (14).

$$Q_s = Q_{SGSC} \tag{14}$$

$$Q_{SGSC} = U_{SGSCq}.\ I_{sd} \tag{15}$$

$$Q_s = \omega_e.\ |\varphi_s|.\ \left(\frac{|\varphi_s|}{L_s} - i_{rd}\right) \tag{16}$$

Substituting (15) and (16) in (14) and considering $I_{sd} = P_m/U_{gd}$ as seen in (5), yields:

$$U_{SGSCq} = \frac{\omega_e.\ |\varphi_s|.\ U_{gd}}{P_m}.\ \left(\frac{|\varphi_s|}{L_s} - i_{rd}\right) \tag{17}$$

The aim is to reach a unitary stator flux, therefore $|\varphi_s| = 1$ must be substituted in (17).

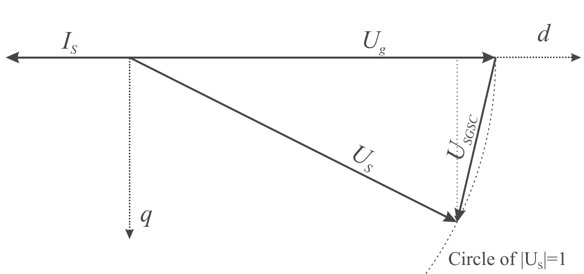

Fig. 2. Space vector diagram of super synchronous operation.

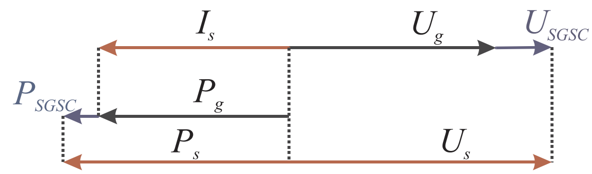

Fig. 3. UPFO for subsynchronous speeds.

$$U_{SGSCq} = \frac{\omega_e.\ U_{gd}}{P_m}.\ \left(\frac{1}{L_s} - i_{rd}\right) \tag{18}$$

The Eq. (18) is used as reference for SGSC control to reach a unitary stator flux.

2.2. Subsynchronous operation

The phasor diagram in Fig. 3 illustrates UPFO at subsynchronous speeds. As can be seen, for this operating condition, the stator voltage needs to be operated above its nominal value, which results in the machine operating at a saturation level. Therefore, it is unviable to operate the machine at subsynchronous speeds with unitary power factor [24,25] and the main purpose of this paper is to find a solution for this drawback.

3. Control design

3.1. Subsynchronous operation

Assuming that DFIG can operate with a power factor different from the unitary, it is possible to reach SGSC power control keeping the module of the stator voltage at its nominal value. Therefore, is proposed to accomplish this task by imposing a phase shift between the grid voltage and the stator voltage. In this case, the machine operates with a unitary power factor, keeping the stator voltage and current aligned, as illustrated in the phasor of Fig. 4 (a).

In Fig. 4 (b), the stator active power is higher than the active power injected into the grid. The difference between P_s and P_g is the active power absorbed by SGSC, where, the active and reactive power of the stator are given by:

$$P_s = U_{sd}.\ I_{sd} \tag{19}$$

$$Q_s = 0 \tag{20}$$

The active and reactive power of DFIG, which are exchanged with the grid are given by:

$$P_{DFIG} = U_{gd}.\ I_{sd} \tag{21}$$

$$Q_{DFIG} = U_{gq}.\ I_{sd} \tag{22}$$

In addition, the active and reactive power of SGSC are given by:

$$P_{SGSC} = P_g - P_s = (U_{gd} - U_{sd}).\ I_{sd} \tag{23}$$

$$Q_{SGSC} = Q_g - Q_s = Q_g - 0 = U_{gq}.\ I_{sd} \tag{24}$$

Although these equations show that it is possible to control SGSC power exchange with the grid by controlling the phases of U_{SGSC} and U_s, simulation results have shown that phase shifts higher than 30° used in SGSC produce distortions in U_s and, as a consequence, electromagnetic torque oscillations.

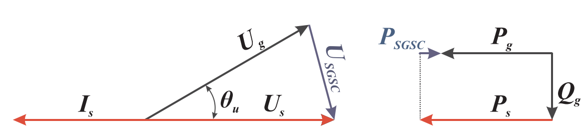

a) Voltages e Current b) Active and Reactive Power

Fig. 4. Phasor diagram of subsynchronous operation.

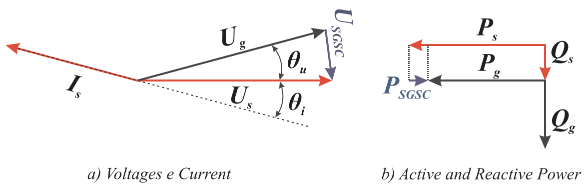

Fig. 5. Phasor diagram of the proposed solution for subsynchronous operation.

Thus, to avoid electromagnetic torque oscillations, the phase shift between the stator voltage and the grid voltage, represented by θ_u in Fig. 4, should be reduced. The proposed solution is to deviate the angle between the stator current and the stator voltage, which can be performed by controlling the RSC. Fig. 5 (a) presents a deviation of the stator current, which is represented by θ_i. Deviating the angle of the stator current allows obtaining the same power absorption by SGSC with a lower phase shift between the stator and the grid voltages, as can be seen in Fig. 5 (b).

Considering the new phase angles, equations of active and reactive power of the stator are given, respectively, by the following equations:

$$P_s = U_{sd}.\ I_{sd} + U_{sq}.\ I_{sq} \tag{25}$$

$$Q_s = U_{sq}.\ I_{sd} - U_{sd}.\ I_{sq} \tag{26}$$

The equations of active and reactive powers of DFIG are given by:

$$P_g = U_{gd}.\ I_{sd} + U_{gq}.\ I_{sq} \tag{27}$$

$$Q_g = U_{gq}.\ I_{sd} - U_{gd}.\ I_{sq} \tag{28}$$

The power equations of SGSC are given by:

$$P_{SGSC} = P_g - P_s = (U_{gd} - U_{sd}).\ I_{sd} + (U_{gq} - U_{sq}).\ I_{sq} \tag{29}$$

$$Q_{SGSC} = Q_g - Q_s = (U_{gq} - U_{sq}).\ I_{sd} - (U_{gd} - U_{sd}).\ I_{sq} \tag{30}$$

Thus, the SGSC power depends on both angles, to θ_u and θ_i. Considering that $|I_s| = |U_s| = |U_g| = 1.0$ p.u., the active power absorbed by SGSC as a function of the angles is presented in Fig. 6.

In Fig. 6, the phase shift of the stator current, θ_i reduces the required phase shift between the stator and grid voltages, θ_u. For example, for a SGSC power of 0.3 p.u. without the stator current phase shift, θ_u must be around 45°, with $\theta_i = 20°$, θ_u is reduced to 30°.

Fig. 7 presents DFIG reactive power as a function of the stator current phase shift, θ_i and phase shift between the stator and grid voltages, θ_u. Considering the example of Fig. 6, despite of the same total DFIG active power, the reactive power is 0.7 p.u. for $\theta_u = 45°$ and $\theta_i = 0°$ while $Q_g = 0.77$ p.u, for $\theta_u = 30°$ and $\theta_i = 20°$. Therefore, deviating not only θ_u but also θ_i slightly increases the total DFIG reactive power.

3.1.1. Analysis under the power curve of a variable speed wind turbine

In order to show the active and reactive power of a wind turbine with a SGSC based DFIG, in which the power processing is made shifting the phases of the stator voltage and current by the SGSC and RSC, the maximum power tracking curve of the aerodynamic model of wind turbine is submitted to equations of the proposed methodology. For such task, first, the power x angular speed curve is submitted to the Eqs. (1) and (2) to obtain the stator active power, rotor active power, and machine slip. The results are given in Fig. 8 for subsynchronous operation.

In Fig. 8, it is possible to see that the rotor active power and the slip decrease as the wind speed increases. On the other hand, the stator active power becomes close to the total DFIG active power as the DFIG becomes closer to the synchronous speeds.

Considering $|U_s| = |U_g| = 1$ and under the limit of θ_u, in which the stator current is still aligned to the stator voltage, the equations of stator and DFIG active power can be written as:

$$P_s = I_s \tag{31}$$

$$P_g = I_s\cos(\theta_u) \tag{32}$$

Therefore by Eqs. (31) and (32) it is possible to obtain I_s and θ_u values until the limit of θ_u. Further, using the limit value of θ_u, the values of θ_i can be obtained by:

$$\theta_i = \tan^{-1}\left(\cot\theta_u - \frac{P_g}{P_s\sin\theta_u}\right) \tag{33}$$

And the stator current is given by:

$$I_s = P_s\cos(\theta_i) \tag{34}$$

With the values of θ_u and θ_i the DFIG reactive power can be calculated by:

$$Q_g = I_s\sin(\theta_u + \theta_i) \tag{35}$$

Using Eqs. (31),(32),(33),(34) and (35) over the values of the Fig. 7, the DFIG reactive power is obtained for maximum values of θ_u of 90°, 30°, and 25°. The results are illustrated in Fig. 9.

As seen in Fig. 9, the lower the limit of θ_u, the higher the DFIG reactive power, due to the higher values of θ_i. Therefore it should be used the higher θ_u possible, which is limited by the distortions in the stator voltage. These distortions have been observed for θ_u slightly greater than 30°, thus a limit of 25° is considered for θ_u. Fig. 10 illustrates the apparent power for different values of θ_u, which is calculated considering the maximum current for subsynchronous operating conditions.

Fig. 10 shows that the reactive power increase provided by the proposed method does not lead the system to operate over the nominal capacity. This is mainly because the proposed control is designed for subsynchronous speeds and, as a consequence, for low power levels absorbed from the wind.

3.1.2. Control system flowchart

In this section, a flowchart is presented in Fig. 11 to illustrate how the decisions are made in the control. As seen, firstly the measured

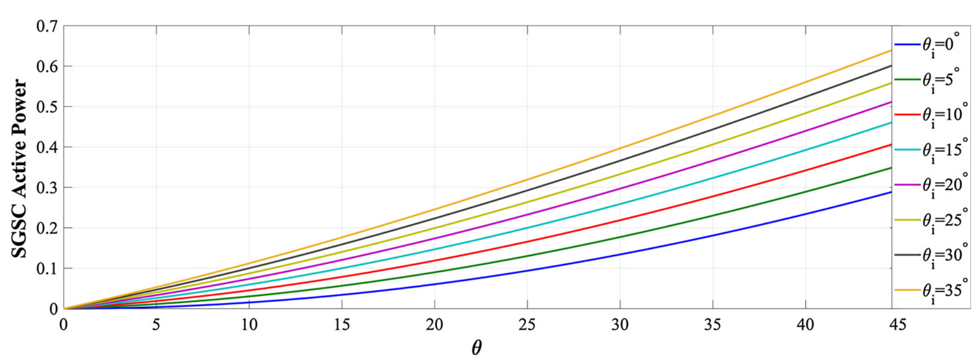

Fig. 6. SGSC active power for different phase angles of voltage and current.

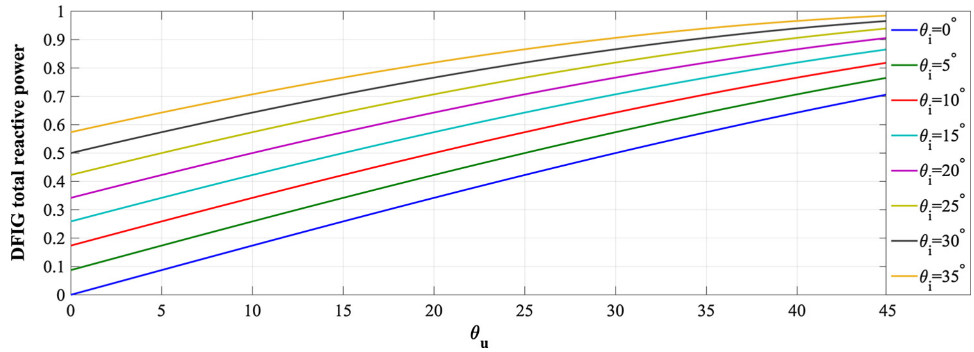

Fig. 7. Total DFIG reactive power.

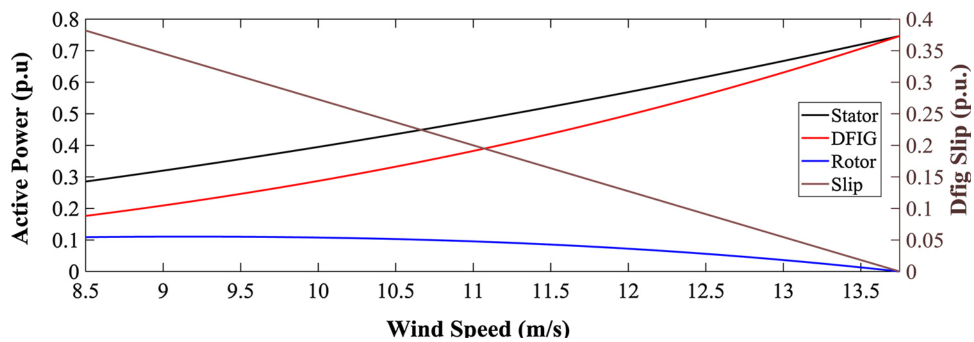

Fig. 8. Active power and slip as a function of wind speed for subsynchronous speeds.

value of the Dc-Link voltage is compared to the reference value and error (delta) is calculated.

If delta is negative, the amount of active power absorbed by the SGSC must be increased. To reach this goal, as seen in Fig. 11, if θ_u is lower than 25° it will be increased, but if θ_u has already reached its limit of 25°, θ_i will be increased.

If delta is positive, the amount of active power absorbed by the SGSC must be decreased. To reach this goal, the opposite procedure is performed, if θ_i is higher than 0°, it will be decreased. Otherwise, θ_u will have to be reduced.

3.2. Reactive power control

The proposed solution results in reactive power exchange between the turbine and the grid. However, current grid codes related to the power factor of wind parks usually require the control of the power factor at the point of common coupling (PCC) in a typical range from 0.92 inductive to 0.92 capacitive.

As a solution, a coordinated control can be applied to the turbines of the wind park to keep a specific power factor at PCC, which is considered a unitary power factor in this paper, but other values can also be used. The coordinated control is managed by the supervisory system, which is commonly available in wind farms and provides the needed communication structure to perform control among wind turbines.

The reference for the control is the reactive power at PCC, and then the reactive power level of each wind turbine is adjusted considering the control of the direct component of SGSC voltage.

In order to perform the reactive power control, the wind farm should be divided into two groups: the first group with a leading power factor and the second one with a lagging power factor, so that the net power factor is the closest possible from required power factor, in this case unitary.

Although it is more convenient that each group presents the same output active power, it is not mandatory. Indeed, to start the process, it is important to know the active power of each group, which can be estimated by the measured wind speed of each turbine in the group or obtained directly from the SCADA system of the wind farm. As the reactive power contribution of the group can be divided by the number of turbines, the groups can have a different number of turbines, which can even operate under different wind speeds.

The control is performed by comparing the measured power factor with the required power factor at PCC. If there is an excess of reactive

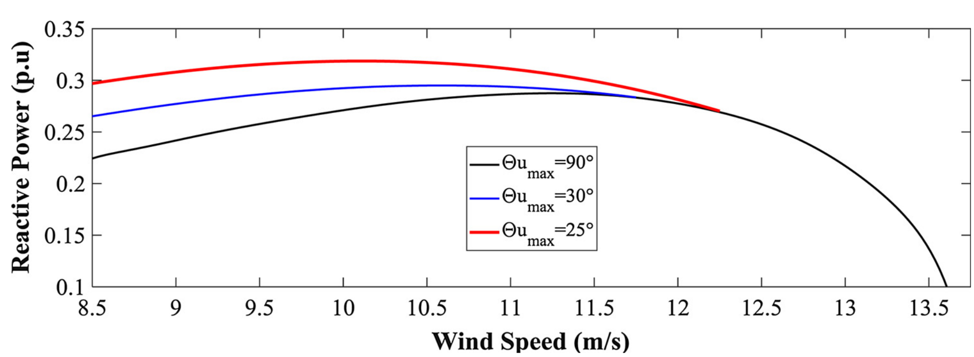

Fig. 9. DFIG Reactive Power x Wind Speed for subsynchronous speeds.

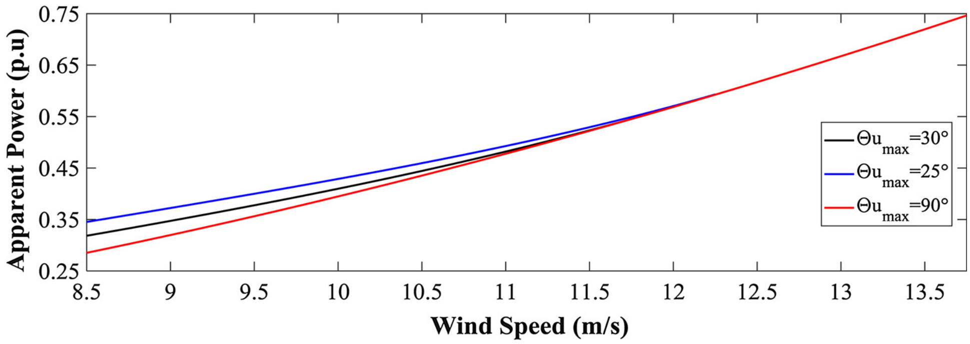

Fig. 10. Apparent Power x Wind Speed for subsynchronous speeds.

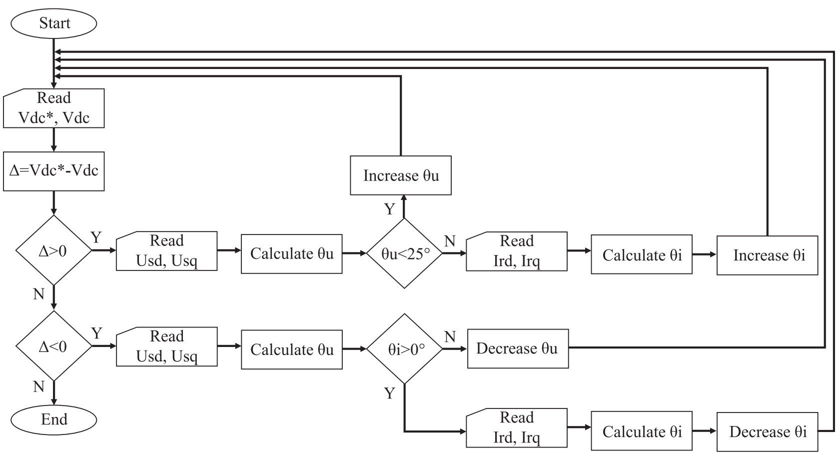

Fig. 11. Subsynchronous power control flowchart.

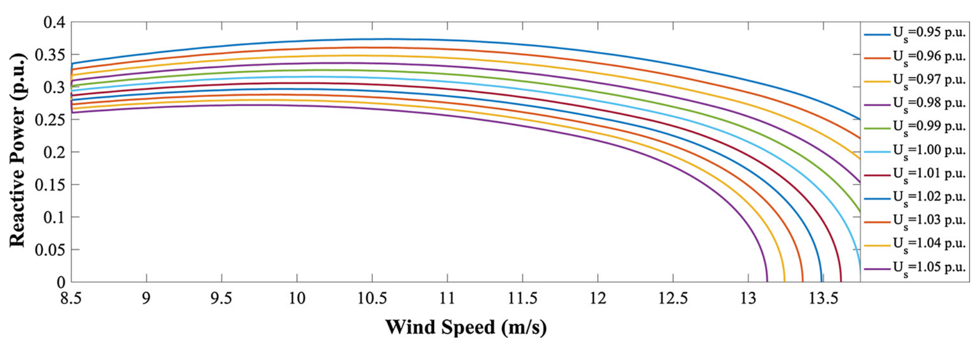

Fig. 12. Impact of stator voltage on the turbine reactive power.

power, the reactive power of the group responsible for injecting reactive power should be reduced. Otherwise, if there is a lack of reactive power, the reactive power of the group responsible for reactive power absorption should be reduced.

In order to decrease the reactive power contribution of a group of turbines, the magnitude of the stator voltage, U_{sd}, should be increased related to U_{gd}. As only a small fraction of the active power of turbines is managed by the reactive power equalization control, changes of the stator voltage magnitudes do not impose a relevant impact on the stator flux.

To illustrate how the SGSC can change the reactive power provided by varying the stator voltage, Fig. 12 brings the same projection of the reactive power by wind speed seen in Fig. 9, considering $\theta_u = 25°$, but varying the stator voltage module in a small range, from 0.95 p.u to 1.05 p.u.

As one can see in Fig. 12, the increase or decrease of the direct component of stator voltage regulates the amount of power that must be absorbed using the phase shift method, therefore the DFIG reactive power changes. As a consequence, increasing the direct component of the voltage in one group of turbines or reducing in the other allows compensating the net reactive power at the PCC.

The main strategy of the coordinated reactive power control is illustrated in the flowchart presented in Fig. 13. When PCC power factor is different from the reference, the control is enabled.

According to the flowchart presented in Fig. 13, firstly the reactive power is obtained from PCC and from each turbine. Q_{pcc} direction is set as the positive reference, therefore, the group of turbines with Q_g aligned with Q_{pcc} will have positive values of reactive power and the group of turbines with Q_g counter-aligned with Q_{pcc} will have negative values of reactive power.

Then turbines with positive values of Q_g will have U_{sd} increased to reduce the reactive power level required for the active power absorption. Turbines with negative values of Q_g will have U_{sd} decreased to increase the reactive power level required for the active power absorption.

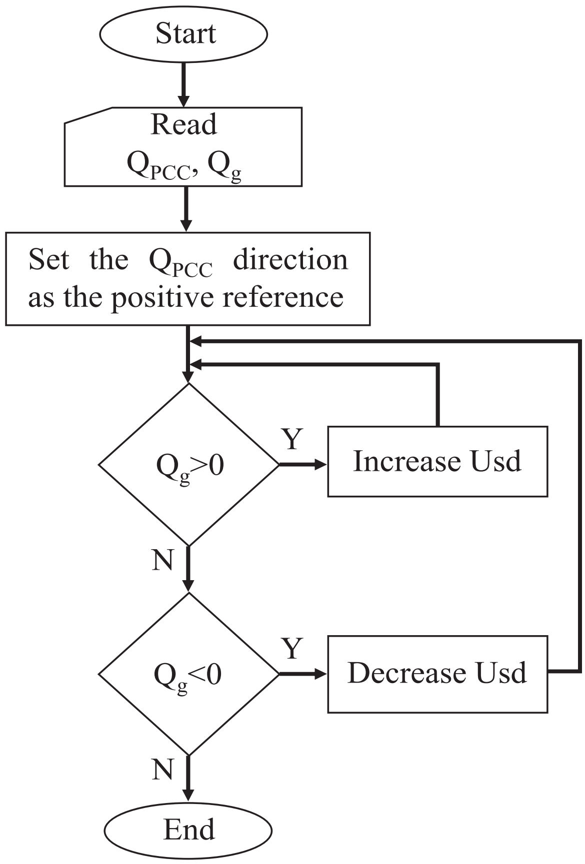

Fig. 13. Coordinated reactive power control flowchart.

3.3. Block diagrams

Figs. 12 and 13 present the control block diagrams of SGSC and RSC. In these controls, the direct axis of the dq0 frame is aligned with the grid voltage.

As one can see in Fig. 14, the reference value of the direct component of SGSC voltage (U_{SGSCd}*) is calculated first to balance the module of the stator voltage ($|U_{sd}|$) to the module of the grid voltage ($|U_g|$), and secondly to absorb or inject active power in the grid modifying the level of active power to be controlled by the phase shifting and balancing the reactive power between both groups of turbines. The quadrature component of the SGSC voltage (U_{SGSCq}*) is responsible for keeping the Dc-Link voltage constant in order to guarantee the correct power flow between the rotor of the machine and the grid.

In Fig. 15, it is possible to notice that the quadrature component of the stator current is only responsible for controlling the DC-Link voltage after θ_u reaches its limit, below this conditions the quadrature control of the RSC just keeps the stator current aligned with the stator voltage. The direct axis control is responsible for the DFIG active power, tracking the curve of best efficiency of the turbine.

It is worth to mention that the controls are applied over the decomposed positive sequence signals, in order to avoid that the negative sequence components of a symmetric or asymmetric fault cause a relevant impact over such controls. As seen in Ref. [19], the decomposition is made by Multiple Second Order Integrators – MSOGI's [36]. Such care is taken, even considering that the operation of the proposed controls under fault is out of the scope of the paper, due to the effect that the decomposition process has to the positive sequence controls. An alternative for such method is the use of Proportional Resonant Controllers – PR's [37].

4. Method validation

In this section, the power processing method is implemented in a model of a Wind Park with turbines employing the SGSC based DFIG's. The test system is presented in Fig. 16. The model is developed using Matlab/Simulink. The aim is to analyze the effects of the method over the parameters of the asynchronous machine and converter.

The modeled test system is composed of seven 2MVA SGSC-based DFIG's, which are connected to PCC by a Y-Δ transformer. The DFIG parameters are presented in Table 1. A load is connected to PCC and a 50 km π-line connects the wind turbines to a 120 kV-system. The 120 kV system is modeled by a transformer, a mutual impedance, and a 120 kV controlled voltage source. A grounding transformer is connected to the 25 kV section to avoid zero-sequence currents flowing in the grid.

The turbines are divided into two groups with slightly different mean wind speeds. The first group, with three turbines, operates at 12.3 m/s mean wind speed and the second group, with four turbines, operates at 13 m/s. Therefore, the angular speed of group 2, identified in the figures by T2, is slightly higher than the angular speed of group 1, identified in the figures by T1, as shown in Fig. 17. Such difference at the number of wind turbines is intentionally chosen to increase the difference in the total power of both groups, as the group with the turbines that operates with higher wind speed has also the higher number of turbines. Therefore, increasing the level of actuation of the Reactive Power Control.

As shown in Fig. 17, the angular speeds of groups 1 and 2 are, respectively, 0.86 p.u. and 0.94 p.u. Likewise, group 2 presents a higher

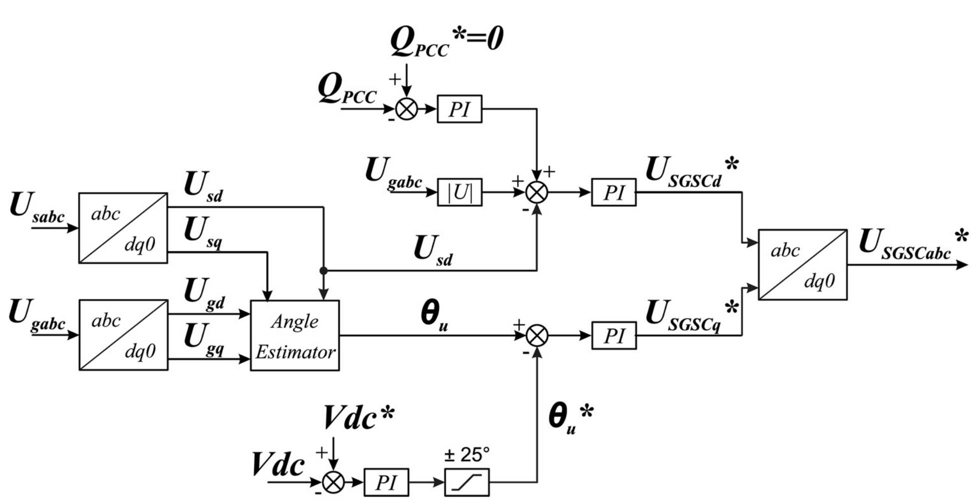

Fig. 14. SGSC control block diagram.

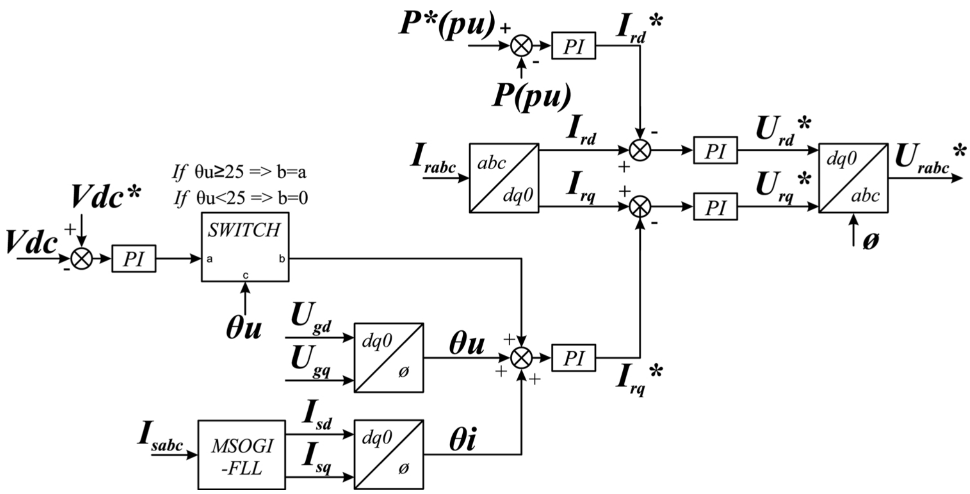

Fig. 15. RSC control block diagram.

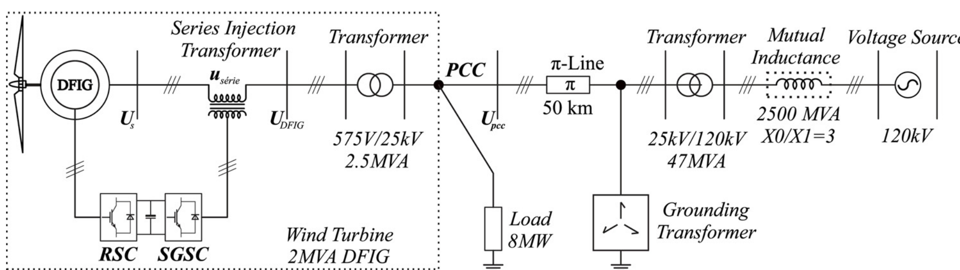

Fig. 16. Test power system configuration with DFIG.

Table 1
DFIG Data.

DFIG Data		
Turbine	Rated wind speed	13.5 m/s
Asynchronous generator	Rated power	2 MVA
	Ratedvoltage/frequency	575 V/60 Hz
	Rs	23 m Ω
	Rr	16 m Ω
	Lls	180 mH
	Llr	160 mH
	Inertia constant	0.685 s
	Pairof poles	3
SGSC	Lc	1.0 mH
	Cc	12000 μF
	Rc	0.5 Ω
DC link	Cdc	45000 μF

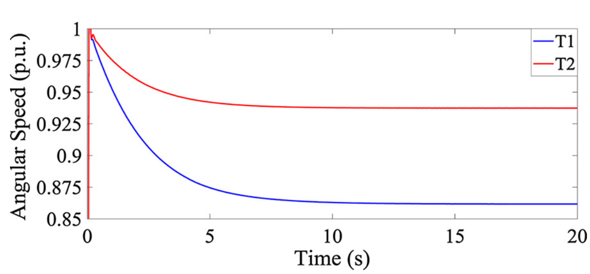

Fig. 17. Angular Speed.

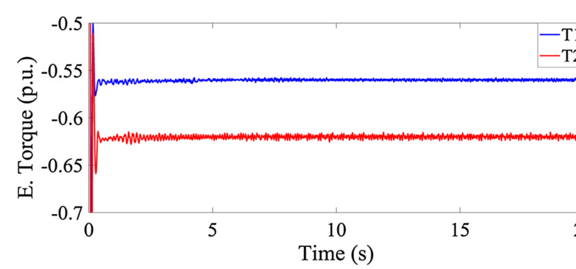

Fig. 18. Electromagnetic Torque.

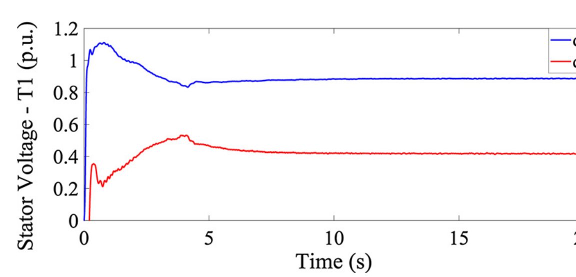

Fig. 19. Stator Voltage - Turbine 1.

electromagnetic torque, which can be seen in Fig. 18. The electromagnetic torque of groups 1 and 2 are, respectively, −0.56 p.u. and −0.62 p.u.

The stator voltages of the turbines, with the *dq0* axis, referred to PCC voltage, are presented in Figs. 19 and 20. Likewise, stator currents, with the *dq0* axis referred to the stator voltage, are presented in Figs. 21 and 22.

The phase shifts of the stator voltages of groups 1 and 2 turbines occur in the opposite direction. Therefore, the reactive power from each group of turbines partially cancels each other. The calculation of angles is performed, after the system reaches the steady state, by the arctangent of q/d relation. The obtained values are 25° leading from PCC voltage for group 1 and 21.5° lagging PCC voltage for group 2.

It is worth to emphasize that the current angles have only deviated from the stator voltage angle when it reaches its limit of 25°. When

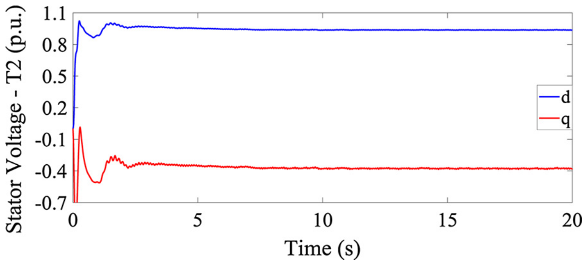

Fig. 20. Stator Voltage - Turbine 2.

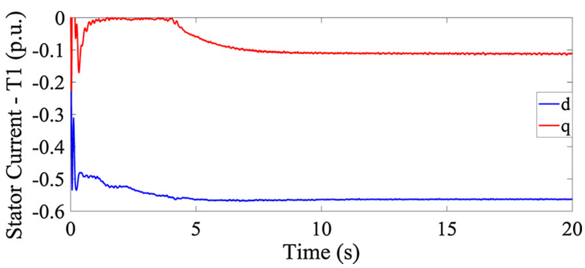

Fig. 21. Stator Current - Turbine 1.

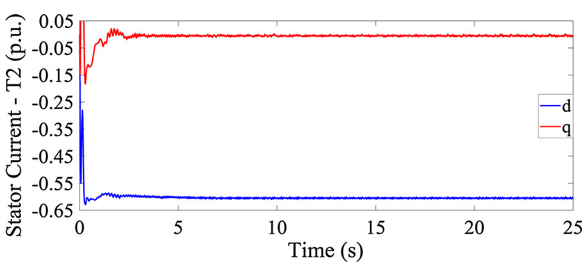

Fig. 22. Stator Current - Turbine 2.

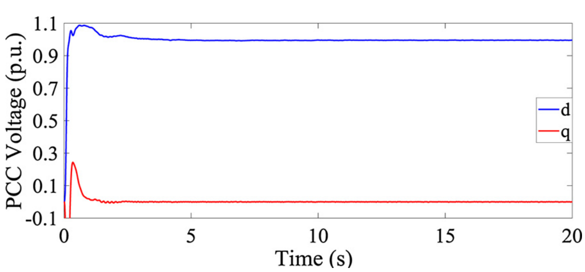

Fig. 23. PCC Voltage.

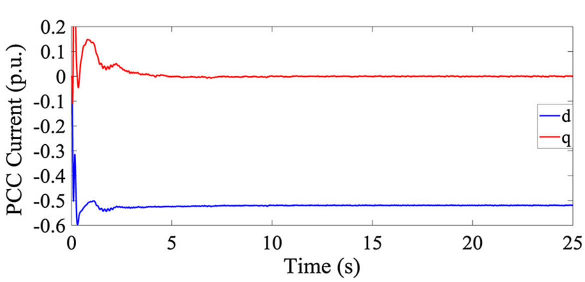

Fig. 24. PCC Current.

calculating the angles of the stator currents of the turbines, using the steady-state values presented in Fig. 22, it is possible to notice that the stator current of group 2 is aligned with the stator voltage, due to the limit of the stator voltage angle deviation that was not achieved. In group 1, the stator voltage angle deviation reaches its maximum, therefore the current has also its angle deviated reaching a phase shift

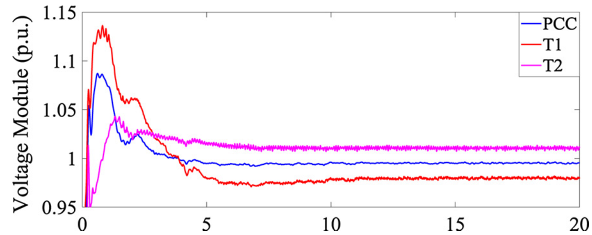

Fig. 25. Voltage Module.

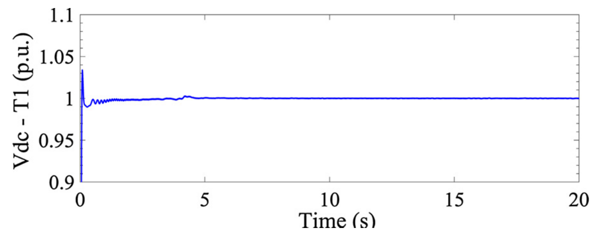

Fig. 26. Dc-Link Voltage - Turbine 1.

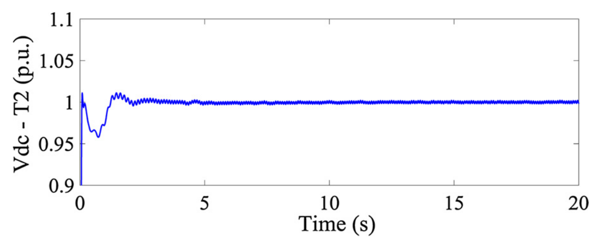

Fig. 27. Dc-Link Voltage - Turbine 1.

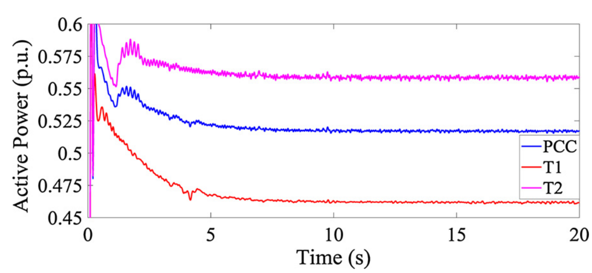

Fig. 28. PCC Active Power.

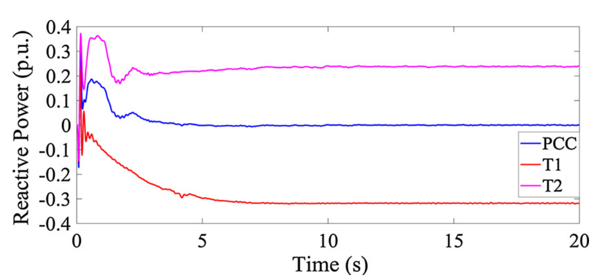

Fig. 29. PCC Reactive Power.

of 11.2°. PCC voltage and current are presented in Figs. 23 and 24.

Figs. 23 and 24 illustrate that reactive power control succeed. The reference for defining *dq0* axis is the PCC voltage, therefore its q component is zero. As the PCC current has also its *q* component equal to zero, is verified the compensation of the reactive power of both groups of turbines.

The control, which keeps the total compensation of the reactive power of both groups of turbines, is performed by changing the modules of the stator voltage of each group of turbines, more specifically

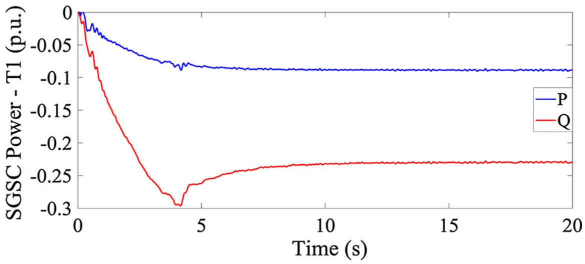

Fig. 30. SGSC Power - Turbine 1.

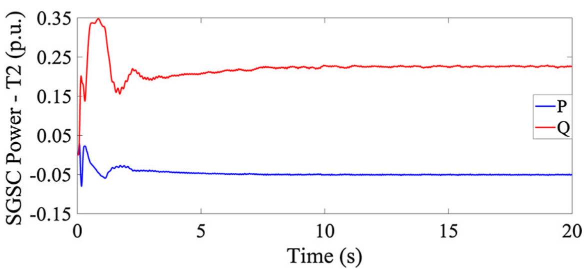

Fig. 31. SGSC Power - Turbine 2.

acting over the direct component, as previously explained. The modules from the stator voltages and of PCC voltage are shown in Fig. 25.

As seen in Fig. 25, group 1 of turbines present the stator voltage magnitude reduced by SGSC in comparison with PCC voltage. Therefore, there is an injection of active power in the grid, increasing the power level to be absorbed by the stator voltage and current angle deviation, consequently, the reactive power exchanged between the turbine and the grid.

The opposite situation occurs with group 2 of turbines. SGSC increases the stator voltage in comparison with PCC voltage. Therefore, absorbing power and reducing the power level to be absorbed by the stator voltage and current angle deviation, consequently the reactive power exchanged between the turbine and the grid. The variation of the stator voltages magnitude, in this case, is ± 0.02 p.u., which does not represent a saturation risk of the stator flux.

Figs. 26 and 27 illustrate the voltages at Dc-Link of the turbines of both groups.

Figs. 26 and 27 show that Dc-Link nominal voltages were successfully maintained by the proposed control method, with constant values after the turbines reach the steady-state operation. It can, therefore, be stated that the posed method succeeds in the power processing task.

Turbines and PCC active and reactive power are presented, respectively, in Figs. 28 and 29. In these figures, PCC active power is the mean value between the values obtained from both groups. It must be highlighted that the base value for PCC active power is two-fold the base value for the stator active power (PCC- 4 MW, Stator-2 MW) and that group two has one turbine more than group one. Therefore, the difference seen in the power from both groups is due to different rated power used, but they indeed are equal as the group 1 needs to have its power multiplied by 3 and the group 2 by 4. Fig. 29 reinforces that the reactive power compensation of the turbines is successful, resulting in no reactive power at PCC.

The SGSC's active and reactive powers from both groups of turbines are shown in Figs. 30 and 31. As seen in the figures, the major part of SGSCs powers is reactive power. Although, the reactive power control allows to compensate such reactive power provided by both groups of turbines, as already demonstrated. The phase opposition between the SGSC reactive powers from the turbines of each group is also seen comparing the Figs. 30 and 31.

5. Conclusion

The use of a SGSC power control based on phase shifts of the stator current and voltage is investigated as a solution for the rotor power managing problem of SGSC-based DFIG when operating at subsynchronous speeds. A coordinated control is also proposed to reduce the reactive power at PCC produced by wind turbines operating out of the unitary power factor.

Simulation studies are provided to validate the proposed solution regarding the aspects of DC-Link voltage maintenance and PCC reactive power control.

Firstly, the results have shown that the proposed method succeeded in controlling SGSC power flux for both groups of turbines operating in different subsynchronous speeds. Considering the period when the turbines are already in the steady state, it is possible to claim that the voltages at DC-Link of the turbines were kept constant at their nominal values and the stator voltage modules have their values near PCC voltage, therefore, avoiding any saturation in the stator flux.

Secondly, the reactive power provided by each group of turbines achieved the proposed reduction at PCC even with the turbines operating at different operational points. Therefore, the opposite phase shift of the stator voltages and currents of each group of turbines, associated with the UPFO-based control to deal with the difference between the reactive powers was effective.

In this context, it is possible to conclude, based on the analyses of the results, that the series-based DFIG configuration tends to be a good solution considering cost, complexity, and voltage hide through capacity.

Among the future perspectives of this work, the response of the series DFIG to symmetrical and asymmetrical faults during subsynchronous operation will be investigated to further explore the benefits of this configuration and the control proposed in this paper.

Aknowledment

This study was financed in part by the Coordenação de Aperfeiçoamento de Pessoal de Nível Superior - Brazil (CAPES) - Finance Code 001, and part by CNPq Project number 438365/2018-6.

References

[1] WWEA - World Wind Energy Association, Publication — WWEA Bulletin Issue 1-2016: Community Wind Special, (2016) [Online]. Available:http://www.wwindea.org/wwea_bulletin_issue_1_2016/ . [Accessed11 July 2018].
[2] WWEA - Wind Energy Association, Press Release — Wind Power Capacity Reaches 539 GW, 52,6 GW Added in 2017, (2018) [Online]. Available: http://www.wwindea.org/2017-statistics/ [Accessed 11 July 2018]..
[3] T. Ackermann (Ed.), Wind Power in Power Systems, John Wiley & Sons, Ltd., Chichester, UK, 2005.
[4] J.G. Njiri, D. Söffker, State-of-the-art in wind turbine control: trends and challenges, Renewable Sustain. Energy Rev. 60 (July) (2016) 377–393.
[5] M. Ezzat, M. Benbouzid, S.M. Muyeen, L. Harnefors, Low-voltage ride-through techniques for DFIG-based wind turbines: state-of-the-art review and future trends, IECON 2013 - 39th Annual Conference of the IEEE Industrial Electronics Society, (2013), pp. 7681–7686.
[6] X. Yingcheng, T. Nengling, Review of contribution to frequency control through variable speed wind turbine, Renew. Energy 36 (June (6)) (2011) 1671–1677.
[7] H.T. Jadhav, R. Roy, A comprehensive review on the grid integration of doubly fed induction generator, Int. J. Electr. Power Energy Syst. 49 (July (49)) (2013) 8–18.
[8] S. Seman, J. Niiranen, A. Arkkio, Ride-through analysis of doubly fed induction wind-power generator under unsymmetrical network disturbance, IEEE Trans. Power Syst. 21 (November (4)) (2006) 1782–1789.
[9] S. Hu, X. Lin, Y. Kang, X. Zou, An improved low-voltage ride-through control strategy of doubly fed induction generator during grid faults, IEEE Trans. Power Electron. 26 (December (12)) (2011) 3653–3665.
[10] Y. Wang, L. Xu, B.W. Williams, Compensation of network voltage unbalance using doubly fed induction generator-based wind farms, IET Renew. Power Gener 3 (March (1)) (2009) 12.
[11] ANSI/NEMA, NEMA - Standards Publication MG1 - 2009: Motors and Generators, (2009).
[12] F.E.V. Taveiros, L.S. Barros, F.B. Costa, Heightened state-feedback predictive control for DFIG-based wind turbines to enhance its LVRT performance, Int. J. Electr. Power Energy Syst. 104 (January) (2019) 943–956.

[13] Y. Kailasa, D. Nanjundappan, V. Boominathan, Enhancement of transient stability of distribution system with SCIG and DFIG based wind farms using STATCOM, IET Renew. Power Gener. 10 (May (8)) (2016) 1171–1180.

[14] H. Rezaie, M.H. Kazemi-Rahbar, Enhancing voltage stability and LVRT capability of a wind-integrated power system using a fuzzy-based SVC, Eng. Sci. Technol. an Int. J. (January) (2019).

[15] H. Shahbabaei Kartijkolaie, M. Radmehr, M. Firouzi, LVRT capability enhancement of DFIG-based wind farms by using capacitive DC reactor-type fault current limiter, Int. J. Electr. Power Energy Syst. 102 (November) (2018) 287–295.

[16] X. Yan, G. Venkataramanan, P.S. Flannery, Y. Wang, Q. Dong, B. Zhang, Voltage-sag tolerance of DFIG wind turbine with a series grid side passive-impedance network, IEEE Trans. Energy Convers. 25 (December (4)) (2010) 1048–1056.

[17] S. Zhang, K.-J. Tseng, S.S. Choi, T.D. Nguyen, D.L. Yao, Advanced control of series voltage compensation to enhance wind turbine ride through, IEEE Trans. Power Electron. 27 (February (2)) (2012) 763–772.

[18] A.O. Ibrahim, T.H. Nguyen, D.-C. Lee, S.-C. Kim, A fault ride-through technique of DFIG wind turbine systems using dynamic voltage restorers, IEEE Trans. Energy Convers. 26 (September (3)) (2011) 871–882.

[19] Jin Yang, J.E. Fletcher, J. O'Reilly, A series-dynamic-resistor-based converter protection scheme for doubly-fed induction generator during various fault conditions, IEEE Trans. Energy Convers. 25 (January (2)) (2010) 422–432.

[20] C. Wessels, F. Gebhardt, F.W. Fuchs, Fault Ride-Through of a DFIG wind turbine using a dynamic voltage restorer during symmetrical and asymmetrical grid faults, IEEE Trans. Power Electron. 26 (March (3)) (2011) 807–815.

[21] A. Darvish Falehi, M. Rafiee, LVRT/HVRT capability enhancement of DFIG wind turbine using optimal design and control of novel PIλDμ-AMLI based DVR, Sustain. Energy, Grids Netw. 16 (December) (2018) 111–125.

[22] R. Sitharthana, C.K. Sundarabalanb, K.R. Devabalajic, S. KumarNataraja, M. Karthikeyan, Improved fault ride through capability of DFIG-wind turbines using customized dynamic voltage restorer, Sustain. Cities Soc. 39 (May) (2018) 114–125.

[23] C.K.W. Schumacher, Active damping of flux oscillations in doublyfed ac machines using dynamic variation of the system's structure, 9th European Conference on Power Electronics and Applications, (2001).

[24] P.S. Flannery, G. Venkataramanan, Evaluation of voltage sag ride-through of a doubly fed induction generator wind turbine with series grid Side converter, 2007 IEEE Power Electronics Specialists Conference, (2007), pp. 1839–1845.

[25] P.S. Flannery, G. Venkataramanan, A fault tolerant doubly fed induction generator wind turbine using a parallel grid side rectifier and series grid side converter, IEEE Trans. Power Electron. 23 (May (3)) (2008) 1126–1135.

[26] P.S. Flannery, G. Venkataramanan, Unbalanced voltage Sag Ride-Through of a doubly fed induction generator wind turbine with series grid-side converter, IEEE Trans. Ind. Appl. 45 (5) (2009) 1879–1887.

[27] B. Singh, V. Emmoji, S.N. Singh, I. Erlich, Performance evaluation of New series connected grid-Side converter of doubly-fed induction generator, 2008 Joint International Conference on Power System Technology and IEEE Power India Conference, (2008), pp. 1–8.

[28] O. Abdel-Baqi, A. Nasiri, Series voltage compensation for DFIG wind turbine low-voltage ride-through solution, IEEE Trans. Energy Convers. 26 (March (1)) (2011) 272–280.

[29] J. Yao, H. Li, Z. Chen, X. Xia, X. Chen, Q. Li, Y. Liao, Enhanced control of a DFIG-Based wind-power generation system with series grid-side converter under unbalanced grid voltage conditions, IEEE Trans. Power Electron. 28 (July (7)) (2013) 3167–3181.

[30] V.P. Suppioni, A.P. Grilo, J.C. Teixeira, Control methodology for compensation of grid voltage unbalance using a series-converter scheme for the DFIG, Electr. Power Syst. Res. 133 (April) (2016) 198–208.

[31] V.P. Suppioni, A.P. Grilo, J.C. Teixeira, Methodology for grid voltage unbalance compensation appling a two-converter series DFIG topology, 2015 IEEE 15th International Conference on Environment and Electrical Engineering (EEEIC), (2015), pp. 1736–1741.

[32] V.P. Suppioni, A.P. Grilo, J.C. Teixeira, Improving network voltage unbalance levels by controlling DFIG wind turbine using a dynamic voltage restorer, Int. J. Electr. Power Energy Syst. 96 (March) (2018) 185–193.

[33] O. Abdel-Baqi, A. Nasiri, Series Voltage Compensation for DFIG Wind Turbine Low-Voltage Ride—Through Solution, IEEE Trans. Energy Convers. 26 (March (1)) (2011) 272–280.

[34] B.B. Ambati, P. Kanjiya, V. Khadkikar, A low component count series voltage compensation scheme for DFIG WTs to enhance fault ride-through capability, IEEE Trans. Energy Convers. 30 (March (1)) (2015) 208–217.

[35] M.J. Morshed, A. Fekih, A new fault ride-through control for DFIG-based wind energy systems, Electr. Power Syst. Res. 146 (May) (2017) 258–269.

[36] P. Rodriguez, A. Luna, I. Candela, R. Mujal, R. Teodorescu, F. Blaabjerg, Multiresonant frequency-locked loop for grid synchronization of power converters under distorted grid conditions, IEEE Trans. Ind. Electron. 58 (January (1)) (2011) 127–138.

[37] Y. Yan, M. Wang, Z.-F. Song, C.-L. Xia, Y. Yan, M. Wang, Z.-F. Song, C.-L. Xia, Proportional-resonant control of doubly-fed induction generator wind turbines for low-voltage ride-through enhancement, Energies 5 (November (11)) (2012) 4758–4778.